Indian Journal of Biochemistry & Biophysics
Vol. 61, December 2024, pp. 804-820
DOI: 10.56042/ijbb.v61i12.12427

Spectroscopic, computational, docking, and cytotoxicity studies on 5-chlorobenzimidazole as a Potent anti-breast cancer agent

VS Kunjumol[1], N Karthik[2], S Sumathi[2] & S Jeyavijayan[2]*

[1]Department of Engineering, University of Technology and Applied Sciences, Shinas, Oman

[2]Department of Physics, Kalasalingam Academy of Research and Education, Krishnankoil-626 126, Tamil Nadu, India

Received 12 July 2024; *revised 19 August 2024*

Benzimidazole derivatives are an important family of drugs because of their biological characteristics and potential for cytotoxicity. In this study, 5-chlorobenzimidazole (5CBZ) computations were performed utilizing the 6-311++G(d,p) basis set and the B3LYP approach. The fundamental frequencies as well as geometric optimization have been determined. The molecule's computed and observed FT-Raman, FTIR, and UV-vis spectra have been compared. Using the charge density distributions that might be correlated to the biological response, the energy gap among HOMO-LUMO and molecule electrostatic potentials has been shown. The overlap population (OPDOS), partial (PDOS), and total (TDOS) densities of states are used to study molecular orbital contributions. Natural Bond Orbital Analysis (NBO) has been utilized to explore numerous inter and intramolecular interactions. Molecular atomic charges have been explored using the Fukui function and Mulliken analysis. The ^{1}H and ^{13}C NMR chemical shifts were calculated with the gauge-independent atomic orbital (GIAO) technique. The likeness of the molecule as drugs has been revealed using molecular docking and ADMET prediction. Further research has been done on the molecule's cytotoxicity and antibacterial properties. Finally, we have identified that the molecule is a favorable pharmacological candidate for anti-breast cancer effects.

Keywords: 5-chlorobenzimidazole, Breast cancer, Cytotoxicity, DFT, Docking

Benzimidazole is a heterocyclic aromatic organic compound with two N atoms on its imidazole ring. The H atom has two tautomer structures since it may migrate quickly from one of the N atoms connected to the imidazole ring to the other N atom in the imidazole ring[1]. Naturally occurring forms of vitamin B12 include benzimidazole and its derivatives[2]. They are a preferred structure in medicinal chemistry and are frequently utilized in the field of pharmacology due to their biological properties[3]. Numerous studies have reported that compounds containing substitutions of benzimidazoles have antimicrobial, antifungal, anti-inflammatory, antiviral, and anticancer effects[4,5]. More attention has been paid to benzimidazole and its derivatives in particular as potential cancer treatments. Because they interact with a variety of negative compounds and show a variety of oxidation states, they open the door to the production of drugs with substantial therapeutic promise in the field of pharmacology. Further, many researchers have investigated the effectiveness of benzimidazole derivatives against cancer cells[6-10]. More recently, research has been done on the 6-bromobenzimidazole for its structural, spectroscopic, NBO, cytotoxicity, and molecular docking investigation using density functional theory (DFT) Approach[11]. In general, DFT has shown to be an effective technique for examining vibrational spectra and biomolecule characteristics. The reason for the great interest in DFT is that it applies to chemical systems faster than conventional quantum mechanical correlation techniques. A careful examination of the literature indicates that 5-chlorobenzimidazole (5CBZ) has not been the subject of a comprehensive theoretical or experimental study. This suggests that spectroscopic investigation be done for 5CBZ utilizing UV-Vis, FT-Raman, and FTIR.

In this study, the highest occupied (HOMO) molecule orbital, lowest unoccupied (LUMO) molecule orbital energies, and molecular electrostatic potential (MEP) of a chemical can be used to learn more about charge transport inside a molecule. The overlap population (OPDOS), total density of states (TDOS) and partial density of states (PDOS) spectra have been combined to study the overlapping of molecular orbitals. To recognize the compound's inter and intramolecular interactions, natural bond orbitals

*Correspondence:
E-mail: sjeyavijayan@gmail.com

(NBO) were also shown. Additionally, Mulliken population analysis and Fukui function calculations have been performed. Utilizing atomic orbital theory, the theoretical ^{13}C and ^{1}H NMR have been determined. A number of biological qualities such as molecular docking, antibacterial activity, cytotoxicity, and ADMET (Absorption, Distribution, Metabolism, Excretion, and Toxicity) properties have been attained. For all of these reasons, 5CBZ was subjected to a thorough vibrational, electrical, and biological examination employing spectroscopic techniques in this work. Spectroscopic data obtained experimentally was supported by DFT calculations. Taking into account the aforementioned factors, the current effort has been performed to provide exhaustive molecular vibrations, geometry and biological factors of the title molecule.

Experimental and Computation

Experimental characterizations

The Sigma-Aldrich sample 5CBZ was utilized directly without further purification. Perkin Elmer's FT-IR spectrometer with a KBr beam splitter, $LiTaO_3$ and He-Ne laser source was used for the FTIR characterization. The sample was made by pressing 5CBZ and KBr into pellet form and then using a BRUKER RFS 27 model interferometer to get the 5CBZ's Fourier transform Raman spectra with a resolution of 2 cm^{-1} at chamber temperature. Wavenumbers between 3500 and 500 cm^{-1} were detected for FT-Raman and FTIR spectra. Using ethanol as a solvent, the UV-Vis spectrophotometer (UV-2600) recorded the UV-Vis spectra of 5CBZ in the wavelength range of 100-450 nm.

Computational details

The Becke's three-parameter exchange functional[12], which enhances the flexibility of the valence electrons, was utilized in all calculations using the Lee-Yang-Parr correlation functional (B3LYP) by the 6-311++G(d,p) basis set. The B3LYP hybrid functional with the 6-311++G(d,p) basis set seemed to be more dependable and produced good results for aromatic compounds when the practical and theoretical parameters were compared[13]. Thus, using the DFT/B3LYP approach with a 6-311++G(d,p) basis set, the electronic wave functions of the molecule 5CBZ have been studied to the best approximation of lowest energy states by Gaussian 09 software[14]. Using 0.9613 as the scaling factor[15] for the B3LYP method, the scaled quantum mechanical (SQM) approach guarantees a satisfactory comparability between the experimental and DFT vibrational frequencies. Sundius' MOLVIB Program (Adaptation V7.0-G77)[16] is employed to calculate the potential energy distribution (PED%) for different frequency modes. The contributions of molecular orbitals in different functional groups of the molecule have been calculated using the Gauss Sum 3.0 software[17]. By merging the results of the GAUSSVIEW software[14] by symmetry attentions, vibrational frequency assignments were produced with a high level of precision. Then, the simulated and observed spectra were utilized and displayed on a similar wavenumber scale for visual comparison.

In this study, Human Progesterone Receptor (PDB ID: 1A28), Human Estrogen Receptor (1ERE), Estrogen Sulfotransferase Receptor (PDB ID: 1AQU) and Epidermal Growth Factor Receptor (PDB ID: 1M17) are the chosen breast cancer proteins that were discovered through Protein Data Bank (http://www.pdb.org)[18]. This study looked into how 5CBZ interacts with breast cancer marker proteins. Using Discovery Studio[19] (2017 R2 client version), we conducted a study of the amino acid and protein structure before performing molecular docking. We utilized PubChem (http://pubch em.ncbi.nlm.nih.gov), one of the public ligand databases[20], to extract the structure of the ligand 5CBZ. Finally, MGL apparatus 1.5.4 and Autodock Vina[21] (Adaptation: 4.2.1) carried out the molecular docking (MD) of 5CBZ with breast cancer markers. The outcomes include projected binding free energy and interactions. In order to discover the pharmacodynamic activities of 5CBZ in our human body, ADMET is a component of a pharmacological profile[22]. There are several online and offline software programs available now to predict drug usage. In this research, we employed the ADMET prediction tool (http://lmmd.ecust.edu.cn/admetsar2/). As a consequence, the ADMET predictions of 5CBZ have been evaluated using the pkCSM-pharmacokinetics web-based tool (http://biosig.unimelb.edu.au/pkcsm/prediction).

Results and Discussion

Molecular structure analysis

The optimized bond quality structure of 5CBZ is shown in (Fig. 1). The optimized global minimum energy for 5CBZ is found as -839.58923891 Hartrees. 5CBZ has C_1 point group, contains chlorine, phenyl and imidazole groups and the bond lengths N1-H14, C2-N3, N1-C2, N3-C9, C5-Cl11 and C7-H13 have

Table 1 — The optimized structural parameters of 5-chlorobenzamidazole

Structural parameters		
Bond length (Å)	B3LYP/6-311++G(d,p)	Experimental[23,24]
N1-C2	1.376	1.374
N1-C8	1.3842	-
N1-H14	1.0073	1.009
C2-N3	1.3053	1.297
C2-H15	1.0807	1.085
N3-C9	1.3874	1.388
C4-C5	1.3853	1.391
C4-C9	1.3987	-
C4-H10	1.0816	1.085
C5-C6	1.4053	1.408
C5-Cl11	1.7634	1.441
C6-C7	1.3896	1.393
C6-H12	1.0822	1.086
C7-C8	1.3934	1.394
C7-H13	1.0835	1.085
C8-C9	1.4137	1.416
Bond angle (°)		
C2-N1-C8	106.7949	-
C2-N1-H14	126.2654	-
C8-N1-H14	126.9397	128.0
N1-C2-N3	113.5023	114.9
N1-C2-H15	121.3256	-
N3-C2-H15	125.1721	125.5
C2-N3-C9	104.87	103.9
C5-C4-C9	117.0371	-
C5-C4-H10	121.7929	121.8
C9-C4-H10	121.17	-
C4-C5-C6	122.8045	121.4
C4-C5-Cl11	118.992	119.4
C6-C5-Cl11	118.2035	-
C5-C6-C7	120.5232	121.5
C5-C6-H12	119.3211	119.3
C7-C6-H12	120.1557	-
C6-C7-C8	117.1455	116.5
C6-C7-H13	120.4919	121.3
C8-C7-H13	122.3626	-
N1-C8-C7	133.2511	-
N1-C8-C9	104.4454	-
C7-C8-C9	122.3035	122.6
N3-C9-C4	129.4264	-
N3-C9-C8	110.3874	110.6
C4-C9-C8	120.1862	-

been calculated at 1.0073, 1.3053, 1.376, 1.3874, 1.7636 and 1.0835 Å, which are in agreement with the experimental XRD values[23,24] of 1.009, 1.297, 1.374, 1.388, 1.441 and 1.085 Å and are illustrated in (Table 1). The angles between C9-N3-C2, N1-C2-N3, C4-C5-Cl11, and N3-C2-H15 are calculated from DFT calculations to be 104.87°, 113.50°, 118.99°, and 125.1°, respectively (Experimental values: 103.9°, 114.9°, 119.4°, and 125.5°). The bond angles of 5CBZ reveal that the small asymmetry is produced by the electronegativity of the chlorine and nitrogen atoms in the ring, as seen in Table 1. Table 2 displays the properties of 5CBZ's thermodynamics. The 5CBZ molecule has an extreme dipole moment of 5.0997 Debye, which denotes a more intense contact between the atoms. Here, 5CBZ is given a total energy of 72.468 Kcal mol^{-1} and a zero-point discrete vibrational energy of 67.88451 Kcal mol^{-1}. These findings are important for understanding how 5CBZ reacts chemically.

Table 2 — The thermodynamic parameters of 5-chlorobenzamidazole

Parameters	DFT-B3LYP/6-311++G(d,p)
Optimized global minimum Energy (Hartrees)	-839.58923891
Total energy(thermal), E_{total} (Kcal mol^{-1})	72.468
Heat capacity, C_v (cal mol^{-1} k^{-1})	29.048
Total Entropy, S (cal mol^{-1} k^{-1})	85.551
Translational Entropy (cal mol^{-1} k^{-1})	40.966
Rotational Entropy (cal mol^{-1} k^{-1})	29.779
Vibrational Entropy (cal mol^{-1} k^{-1})	14.805
Vibrational energy, E_{vib} (Kcal mol^{-1})	70.691
Zero-point vibrational energy, (Kcal mol^{-1})	67.88451
Rotational constants (GHz)	
A	3.40304
B	0.72038
C	0.59452
Dipole moment (Debye)	5.0997

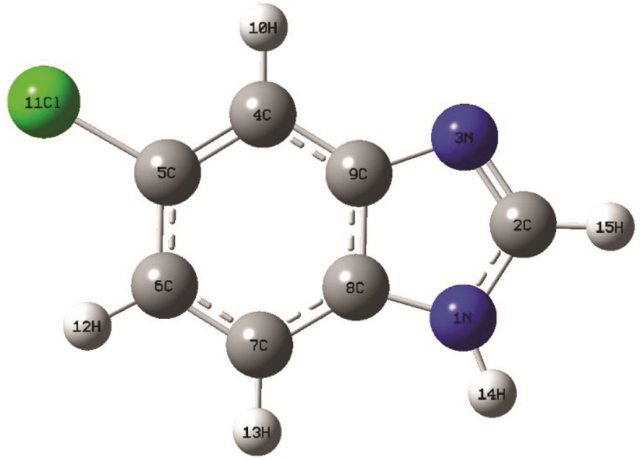

Fig. 1 — Optimized structure of 5-chlorobenzamidazole

Vibrational Assignments

There are 39 normal vibrations in 5CBZ that are active since it contains 15 atoms, as shown by its FT-Raman and FT-IR vibrational spectra. The estimated and experimentally observed FTIR and FT-Raman spectra of 5CBZ are given in (Figs 2 and 3).

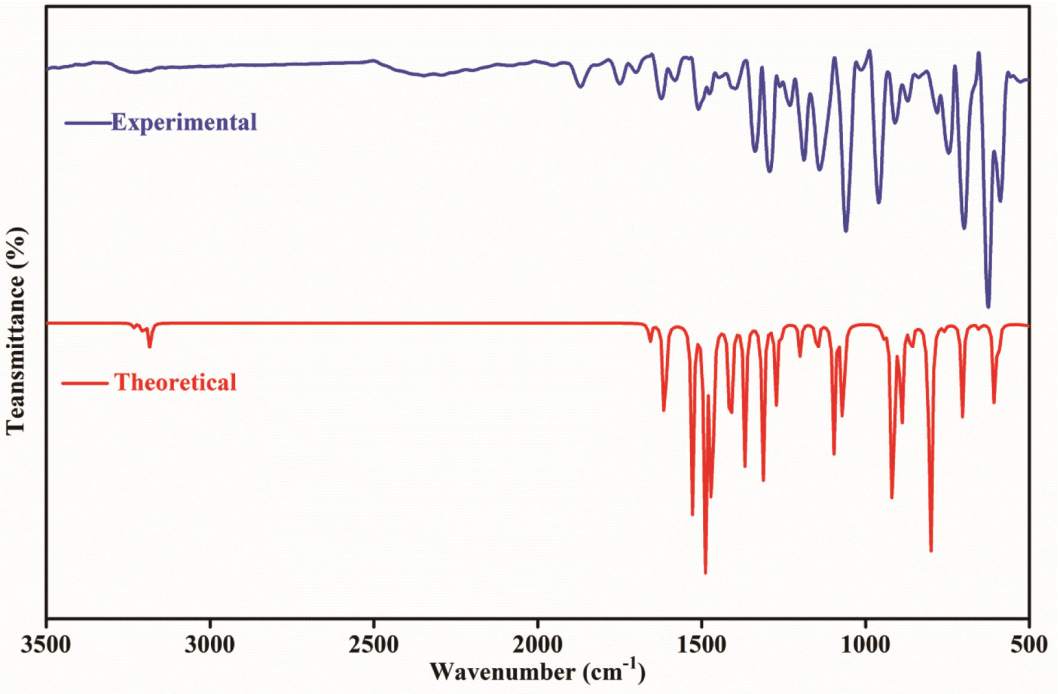

Fig. 2 — FTIR spectrum of 5-chlorobenzamidazole

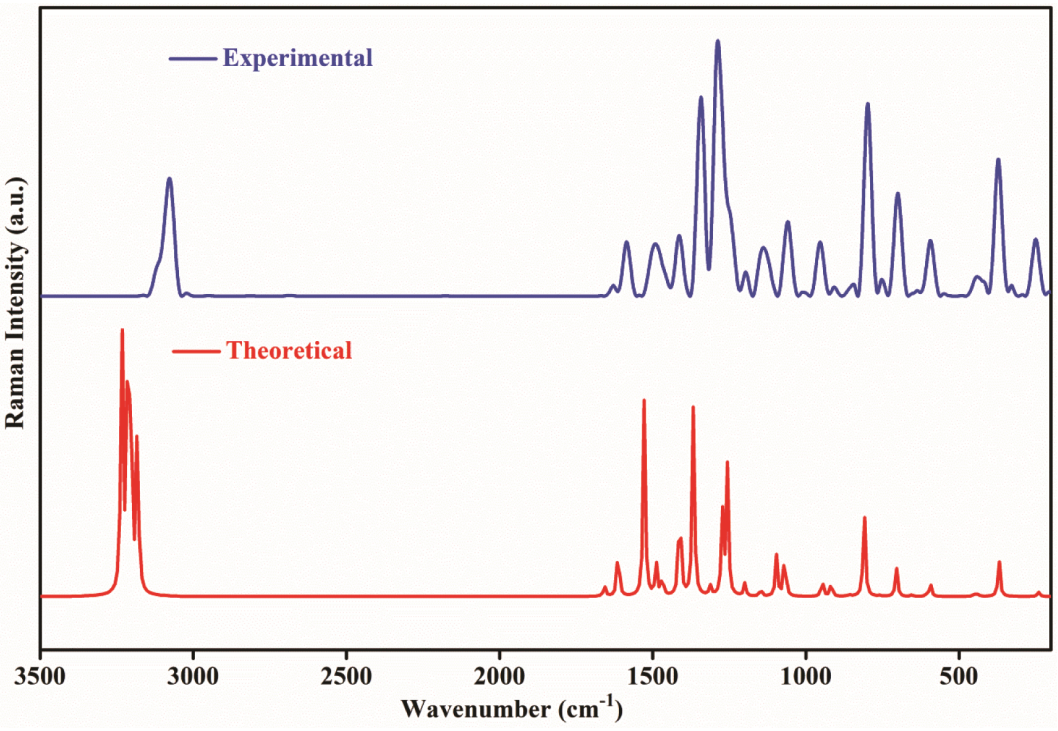

Fig. 3 — FT-Raman spectrum of 5-chlorobenzamidazole

In Table 3, the PED% is used to depict the intensities and vibrational assignment of 5CBZ. The N-H stretching vibrations are seen in the 3500–3300 cm^{-1} range for heterocyclic compounds[25]. This weaker band of the FTIR spectrum for the stretching N-H vibration of 5CBZ is therefore measured at 3500 cm^{-1} (99% PED), and its predicted value is measured at 3517 cm^{-1}. The range between 1350 and 1250 cm^{-1} is where the in-plane N-H deformation is anticipated, and this mode is ascribed to the band at 1235 cm^{-1} in

Raman, 1252 cm^{-1} in the FTIR, and at 1223 cm^{-1} in theoretically, as well as the out-of-plane N-H at 833 cm^{-1} for 5CBZ. The scaled frequencies at 3108, 3091, 3081 and 3059 cm^{-1} (over 90% PED) are attributed to the C-H vibrations of 5CBZ because the C-H stretching vibrations[26] are built up in the range of 3100 and 3000 cm^{-1}. In FTIR, the relevant experimental frequencies were detected at 3105, 3088 and 3083 cm^{-1}, while in FT-Raman; they were discovered at 3077 and 3050 cm^{-1}. The crucial role of the C-C stretching wavenumbers[27] in the substituted aromatic molecules is depicted in the range of 1430–1650 cm^{-1}. Hence, the experimental peaks in 5CBZ are assigned to C-C vibrations with 80–85% PED at 1581, 1510, 1477, 1396 cm^{-1} in the IR and 1585, 1565, 1491, 1439, 1413, 1342 cm^{-1} in the Raman. In aromatic compounds, the three or four bands of the C-N stretching vibrations occur between 1670 and 1320 cm^{-1}. Socrates[28] asserts that the types of ring atoms and substituents, as well as their

Table 3 — The vibrational assignments based on PED calculations for 5-chlorobenzamidazole

S. No	Observed wave number (cm^{-1})		Wave number (cm^{-1})		IR Intensity (Km mol^{-1})	Raman activity ($Å^4$ amu^{-1})	Reduced mass(amu)	Force constant (mDyne/$Å^{-1}$)	Assignment with PED (%)
	FT-IR	FT- Raman	Calculated	Scaled					
1	3500(vw)	-	3658.34	3517	79.3986	149.1831	1.0812	8.5254	νNH(99)
2	3105(vw)	-	3233.39	3108	0.8748	140.2999	1.0972	6.7584	νCH(98)
3	3088(vw)	-	3215.13	3091	0.1074	86.1336	1.0927	6.6552	νCH(97)
4	3083(vw)	3077(ms)	3204.52	3081	2.1370	125.7179	1.0941	6.6198	νCH(93)
5	-	3050(vw)	3182.14	3059	5.2355	85.1705	1.0896	6.5005	νCH(92)
6	1581(w)	1585(ms)	1657.89	1593	3.6201	3.6310	6.8438	11.0830	νCC(85)
7	1510(w)	1565(vw)	1612.82	1550	24.9910	17.7569	6.8608	10.5147	νCC(83)
8	1477(ms)	1491(ms)	1527.87	1469	33.0605	62.8385	4.4755	6.1555	νCC(80)
9	-	1439(vw)	1488.94	1431	43.9744	10.3415	4.1269	5.3905	νCC(84)
10	-	1413(ms)	1468.75	1412	46.4803	6.1980	2.5778	3.2764	νCC(81)
11	1396(vw)	1342(vs)	1411.88	1357	29.5689	33.9092	2.7813	3.2666	νCC(80)
12	1336(ms)	-	1367.45	1315	25.2221	59.1909	3.2107	3.5374	νCN(74)
13	1292(s)	1287(vs)	1312.80	1262	28.5162	2.9828	3.6405	3.6967	νCN(72)
14	1252(vw)	1235(vw)	1272.52	1223	14.3489	25.1071	1.7092	1.6307	bNH (72)
15	1230(w)	1210(w)	1256.14	1208	1.6304	39.0608	2.1936	2.0393	νCN(72)
16	1188(ms)	-	1199.62	1153	5.8903	3.7553	2.1096	1.7887	νCN(72)
17	1139(ms)	1139(ms)	1147.52	1103	6.9344	2.1367	1.5112	1.1724	bCH (76)
18	1058(vw)	1059(ms)	1096.17	1054	22.6397	11.9789	1.7386	1.2308	bCH (77)
19	1014(vw)	1032(vw)	1069.07	1028	24.2818	13.2537	2.0478	1.3789	bCH (75)
20	960(vw)	953(vw)	946.78	910	2.0489	4.8524	6.4104	3.3856	bCH (73)
21	910(ms)	915(vw)	941.07	905	0.3363	0.0833	1.3126	0.6849	ωCH (65)
22	871(vw)	-	917.02	882	47.1233	4.1109	5.7589	2.8533	ωCH (63)
23	853(vw)	850(vw)	890.41	856	22.5803	0.0149	1.4621	0.6830	ωCH (63)
24	840(vw)	833(vw)	859.47	826	5.9587	0.4723	1.4079	0.6127	ωNH(62)
25	781(vw)	798(s)	809.47	778	11.0305	24.4173	5.0923	1.9660	ωCH (63)
26	746(ms)	755(vw)	799.86	769	38.3672	0.0694	1.4569	0.5492	R_1asymd(67)
27	700(vw)	-	758.80	729	0.9776	0.2128	4.5083	1.5294	R_1symd(65)
28	624(vw)	699(s)	704.41	677	16.6726	7.5266	7.6703	2.2424	R_1trigd(65)
29	598(vw)	593(ms)	653.66	589	1.1234	0.4077	3.2709	0.8234	R_2asymd(67)
30	588(ms)	580(vw)	606.38	583	15.9583	0.3710	2.7876	0.6039	R_2symd(66)
31	550(vw)	-	594.03	571	4.6504	3.6345	6.6708	1.3869	νCCl(72)
32	470(vw)	453(vw)	451.59	434	6.6518	0.5733	4.7606	0.5720	tR_2asymd(58)
33	451(vs)	440(vw)	442.69	426	92.3262	0.6677	1.3519	0.1561	tR_2asymd(57)
34	422(vw)	410(vw)	430.46	414	7.6327	0.1589	2.8551	0.3117	tR_1symd(58)
35	-	372(ms)	369.29	355	4.0244	9.4917	12.7698	1.0261	tR_1asymd(60)
36	-	320(vw)	329.10	316	4.5513	0.0379	6.3057	0.4024	tR_1trigd(60)
37	-	249(ms)	241.42	232	1.1305	1.0910	9.0421	0.3105	bCCl(61)
38	-	223(vw)	234.63	226	0.8793	0.1032	5.0722	0.1645	ωCCl(57)
39	-	115(ms)	122.41	118	3.7486	0.8475	6.8342	0.0603	Butterfly(55)

w-weak, s-strong, m-medium, vs-very strong, ν-stretching; b-in-plane bending, ω-out of plane bending, t-torsion, R-ring

positions, affect the intensities of these bands. Strong bands seen in 5CBZ at 1336 cm^{-1}, 1292 cm^{-1} in the IR, and 1287 cm^{-1} in Raman were attributed to the C-N stretching modes (72–74% PED). In the 760-505 cm^{-1} range, the C-Cl stretching vibrations often result in strong bands[23]. In the current analysis, the strong band at 550 cm^{-1} in the IR spectra was found to originate from the C-Cl stretching mode of 5CBZ. In the range between 450 and 250 cm^{-1}, the C-Cl in-plane bending modes typically exhibit strong to medium intensity. The in-plane bending of 5CBZ was identified at 249 cm^{-1} in the Raman spectra. The out-of-plane bending mode of 5CBZ by C-Cl was detected at 223 cm^{-1}. Five extremely strong bands seen in the IR spectra of 5CBZ at wavelengths of 746, 700, 624, 598 and 588 cm^{-1} were attributed to ring in-plane bending vibrations. Raman bands at 755, 699, 593 and 580 cm^{-1} all show the same vibration. Ring vibrations that bend out of plane are observed between 445 and 355 cm^{-1} and the majority of monosubstituted imidazoles show medium intensity bands[11]. In the Raman spectrum at 453, 440, 410, 372 and 320 cm^{-1} as well as in the IR spectrum at 470, 451 and 422 cm^{-1} bands were identified for 5CBZ as rings out of plane bending vibrations. The literature reports are also helped to identify the in-plane and out-of-plane bending vibrations for all normal modes, and they are shown in (Table 3).

Frontier molecular orbitals and DOS spectra

The quantum chemistry parameters such as HOMO, LUMO, and border orbital gap serve as examples of kinetic stability and chemical reactivity of the molecules[29]. At B3LYP/6-311++G(d,p) in 5CBZ, HOMO and LUMO energies as well as the orbital energy gap were calculated. The outcomes of the computations are shown in (Table 4). Figure 4 shows a

Table 4 — Molecular orbital contributions of 5-chlorobenzamidazole

TD-DFT/ B3LYP/6-311++G(d,p)

Energy(eV)	Oscillator strength	Computed wavelength (nm)	Experimental wavelength(nm)	Major contributions	Assignment
4.5928	0.0325	269.95	-	H-1→ L (43.08%)	π→π*
4.7844	0.0924	259.14	-	H → L (51.03%)	π→π*
4.9435	0.0009	250.80	257.72	H-2→ L (97%)	π→π*

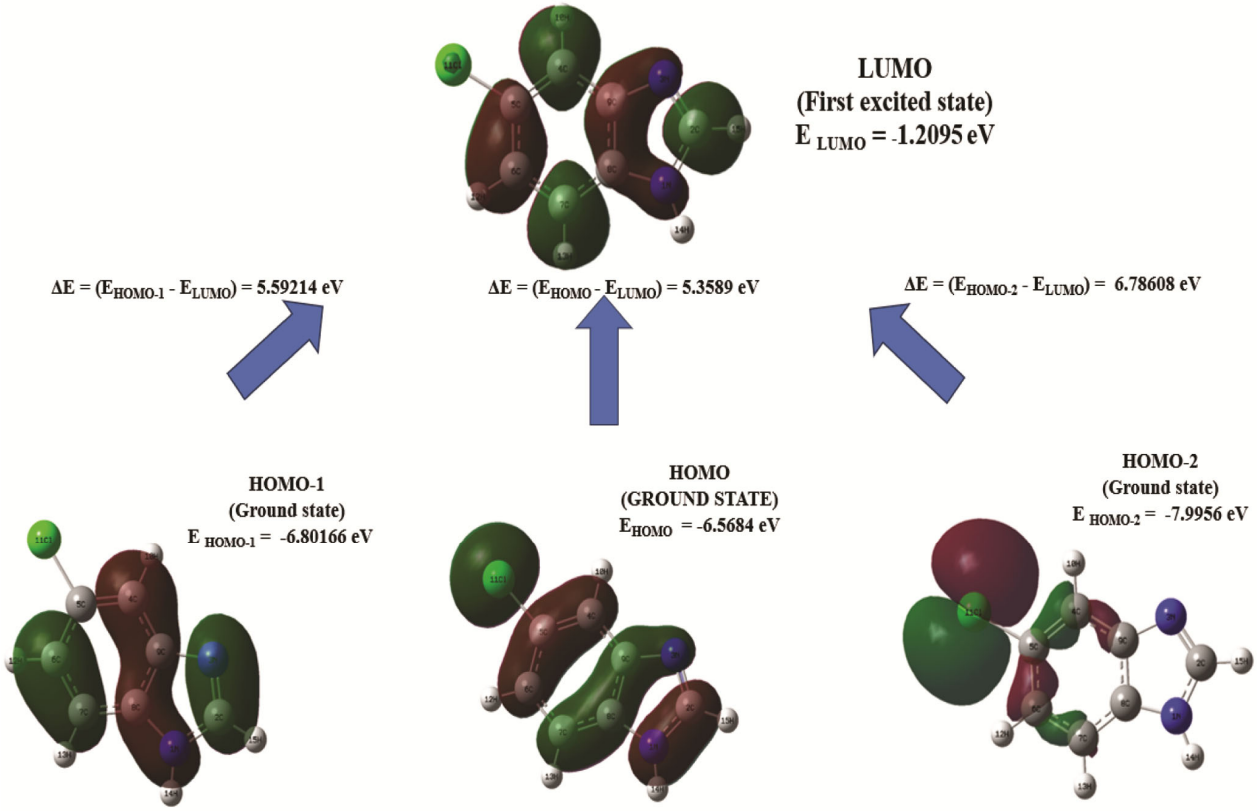

Fig. 4 — HOMO-LUMO plot of 5-chlorobenzamidazole

3D rendering of the border orbitals of 5CBZ. According to calculations, the HOMO energy is -6.5684 eV, which enables chlorine atom in the ring to act as the electron donor. The energy gap is determined to be 5.3589 eV since the LUMO, which has an energy of -1.2095 eV, is situated above the C-C bond of the ring (the leading electron acceptor). Figure 5 shows the UV-Visible plot of 5CBZ, which also displays the observed absorption peaks at 257.72 nm and the equivalent predicted peak at 250.80 nm. This means that, as stated in Table 4, the maximum H-2→L contribution is 97%. Table 5 lists the important global reactivity descriptors for 5CBZ determined using the B3LYP/6-311++G(d,p) approach utilizing Koopman's relations[30]. To verify the stability order of molecular systems, the hardness (η), electronegativity (χ) and chemical potential (μ) are the essential parameters. The definition of electronegativity (χ) is the opposite of the chemical potential. The chemical hardness will be a good indicator of the chemical stability. Hard molecules have a significant energy gap compared to soft molecules' modest energy gap[31]. In the gas phase, the chemical hardness and softness of 5CBZ are determined to be 2.6794 eV and 0.187 eV^{-1}, respectively.

It's possible for neighboring orbitals in a border zone to have identical degenerate energy levels. If this is the case, describing border orbitals only in terms of HOMO and LUMO may not be appropriate. For this reason, overlap population density of states (OPDOS), (also known as COOP- Crystal Orbital Overlapping Population) are the sum of alpha (α) and beta (β) electron density of states[32], created by combining the molecular orbital data with Gaussian curves using the GaussSum 3.0 program. Figure 6 illustrates how the makeup of a molecule's orbitals affects the chemical bonds of 5CBZ. The density of state plot is used to show how the system's energy gap and border orbitals are composed. PDOS displays the contribution of particular atoms or functional groups to each molecular orbital. We may use relevant fragments to assess non-bonding, bonding and anti-bonding features using OPDOS. In OPDOS graphs show bonding interactions as positive values, anti-bonding interactions as negative values, and non-bonding interactions as values close to zero. A total of 78 electrons are occupied in DOS of 5CBZ, which contains both 39α and 39β electrons. As a result, in the 5CBZ structure, interactions between carbon and hydrogen atoms exhibit bonding, whereas interactions between chlorine and carbon atoms, nitrogen and carbon atoms exhibit anti-bonding, as illustrated in the COOP diagram (Fig. 6).

Table 5 — Global reactivity descriptors for 5-chlorobenzamidazole

Molecular Properties	B3LYP/6-311++G(d,p)
HOMO (eV)	-6.5684
LUMO (eV)	-1.2095
ΔE (E_{HOMO} -E_{LUMO}) (eV)	5.3589
Ionization potential (I) (eV)	6.5684
Electron affinity (A) (eV)	1.2095
Global hardness (η) (eV)	2.6794
Global softness (s) (eV^{-1})	0.187
Electronegativity (χ) (eV)	1.2095
Chemical potential (μ) (eV)	-1.2095
Global electrophilicity (w) (eV)	2.8222

Natural bond orbital analysis

In-depth information regarding inter and intramolecular bonding as well as charge interchange in every molecular system is provided by NBO analysis[33]. The donor-acceptor stabilization energies of 5CBZ are recorded in (Table 6) together with the

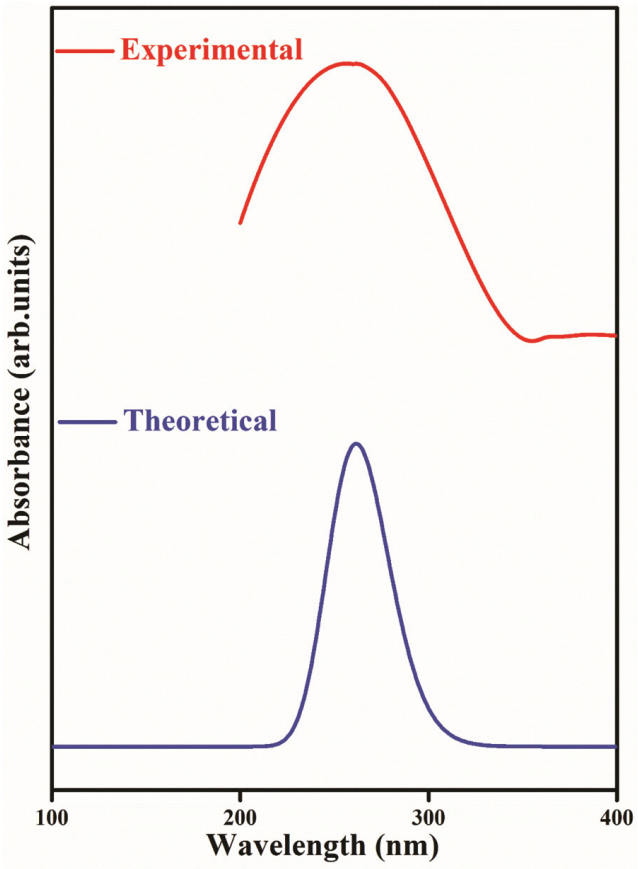

Fig. 5 — UV plot of 5-chlorobenzamidazole

results of the DFT/B3LYP/6-311++G(d,p) computation for NBO research to assess the delocalization interactions. ED(i) and ED(j) represent the stabilizing donor and acceptor interaction over the bound atom. An empty or full bonding, an anti-bonding, or a lone pair can be a donor, whereas a filled bonding or a lone pair can be an acceptor. These contacts are necessary for a relationship to be strong. The bond will be strengthened if the contact is in a bonding pair, but it will be diminished if a lone pair acts as the donor or acceptor[33]. The molecule's distinguishing feature for biological applications is identified by its greater stabilization energy between and π to π*. In 5CBZ, the orbitals with the highest stabilization energies are π(C6-C7)→π*(C8–C9), π(C4-C5) →π*(C6–C7) and π(C8-C9)→π*(C4–C5) (20.24, 20.56, and 23.10 Kcalmol^{-1}) orbitals. The significant delocalization is shown by the strong interaction inside LP(1)N1 and the antibonding orbital π*(C2-N3) having 45.13 Kcalmol^{-1}. Chlorine and nitrogen atoms have strong hyper conjugative interactions with the ring structure, which causes a considerable decrease in lone pair electron density when compared to other orbitals.

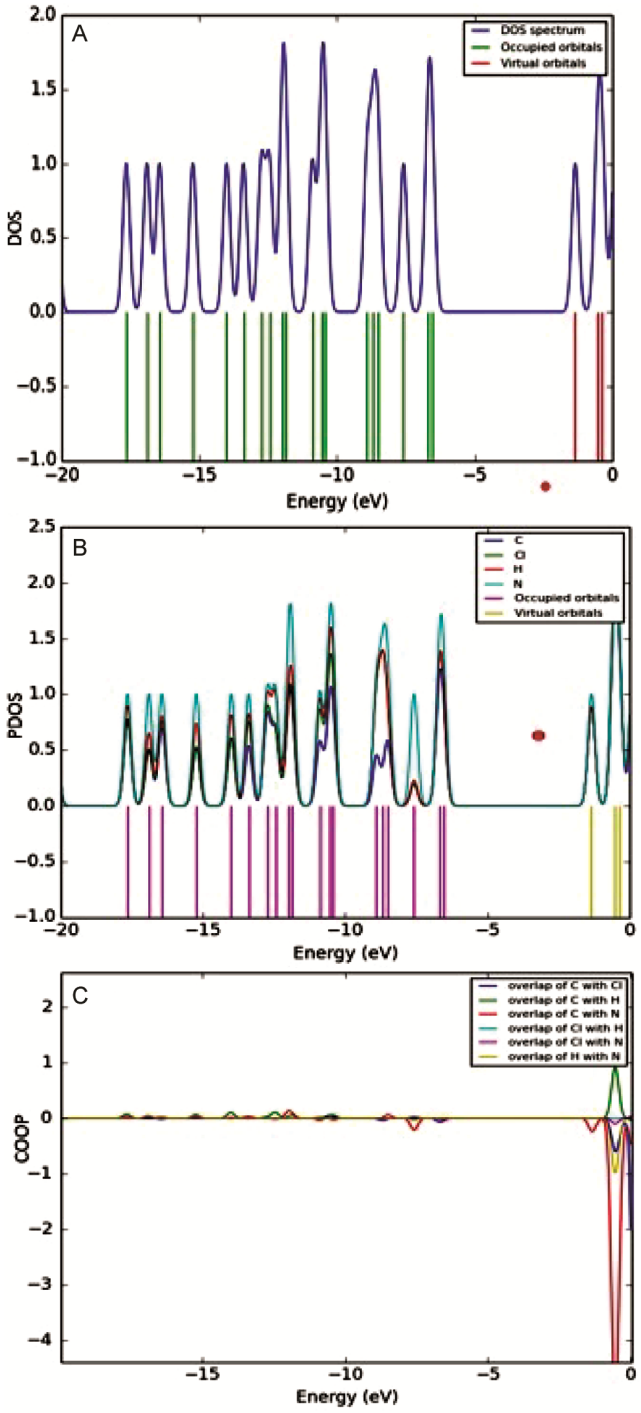

Fig. 6 — (A) DOS; (B) PDOS; and (C) COOP Spectra of 5-chlorobenzamidazole

Mullikan charge electronic analysis

Mulliken charges study intersects electronic gathering and dipolemoment, which gives it a dynamic role in the chemical system[34]. Figure 7 and Table 7 both show the sharing of charges in 5CBZ using the B3LYP and 6-311++G(d,p) basis set. Here, all the nitrogen atoms (N1, N3) have negative charges whereas all the hydrogen atoms (H10, H12, H13, H14, and H15) and chlorine (Cl11) (0.37728) atoms have positive charges. The carbon C6 atom (-1.15987) has the greatest negative charge matched to the other negative carbon atoms, making it a donor atom, since C6 is attached near to chlorine atom (Cl11). Similarly, the carbon C5 atom (0.742644) has the most positive charge compared to the other atoms due to surrounding nitrogen atom (N3), making it an acceptor atom.

Fukui function

Fukui indices, also known as reactivity indices, provide information about the likelihood of an atom within a molecule losing or accepting an electron, which chemists interpret as indicating a greater likelihood of the atom being attacked by either a nucleophilic or an electrophilic attack. Fukui function has been determined from the individual atomic charge using Mulliken population analysis. Usually Fukui function[35] is calculated by:

$$f_k^+ = q_j(N+1) - q_j(N)$$

$$f_k^- = q_j(N) - q_j(N-1)$$

Table 6 — Second-order perturbation theory analysis of Fock matrix for 5-chlorobenzamidazole

Donor(i)	ED (i) (e)	Acceptor (j)	ED (j) (e)	Stabilization energyE(2)(Kcal/mol)	Energy differenceE (j) −E (i) (arb. units)	Fock matrix element F(i,j)(arb. units)
σ(C2-N3)	1.98319	σ*(C4-C9)	0.01938	4.03	1.35	0.066
π(C2-N3)	1.88579	π*(C8-C9)	0.48986	15.09	0.30	0.067
σ(C4-C5)	1.97579	σ*(N3-C9)	0.02115	5.83	1.10	0.072
π(C4-C5)	1.69775	π *(C6-C7)	0.35975	20.56	0.28	0.069
π(C4-C5)	1.69775	π*(C8-C9)	0.48986	19.50	0.28	0.069
σ(C4-C9)	1.97104	σ*(C5-Cl11)	0.02898	4.31	0.87	0.055
σ(C4-H10)	1.97631	σ*(C5-C6)	0.02697	4.10	1.08	0.060
σ(C4-H10)	1.97631	σ*(C8-C9)	0.03421	4.41	1.01	0.060
σ(C6-C7)	1.96475	σ*(N1-C8)	0.02751	7.22	1.04	0.077
σ(C6-C7)	1.96475	σ*(C5-Cl11)	0.02898	4.77	0.84	0.057
π(C6-C7)	1.69468	π*(C4-C5)	0.39464	19.59	0.27	0.067
π(C6-C7)	1.69468	π*(C8-C9)	0.48986	20.24	0.27	0.069
σ(C6-H12)	1.97762	σ*(C4-C5)	0.02573	4.50	1.08	0.062
σ(C7-H13)	1.97904	σ*(C8-C9)	0.03421	4.15	1.02	0.053
σ(C8-C9)	1.96667	σ*(C7-C8)	0.01879	4.02	1.25	0.063
π(C8-C9)	1.56065	π*(C2-N3)	0.32468	13.92	0.22	0.051
π(C8-C9)	1.56065	π*(C4-C5)	0.39464	23.10	0.26	0.070
π(C8-C9)	1.56065	π*(C6-C7)	0.35975	22.37	0.27	0.070
LP(1)N1	1.63296	π*(C2-N3)	0.32468	45.13	0.25	0.096
LP(1)N1	1.63296	π*(C8-C9)	0.48986	25.27	0.29	0.079
LP(1) N3	1.94117	σ*(N1-C2)	0.02646	5.42	0.77	0.058
LP(1) N3	1.94117	σ*(C8-C9)	0.03421	4.22	0.88	0.055
LP(2)Cl11	1.97134	σ*(C4-C5)	0.02573	4.19	0.86	0.054
LP(2)Cl11	1.97134	σ*(C5-C6)	0.02697	4.16	0.88	0.054
LP(3)Cl11	1.93301	π*(C4-C5)	0.39464	12.09	0.33	0.061
π*(C2-N3)	0.32468	π*(C8-C9)	0.48986	33.06	0.04	0.051

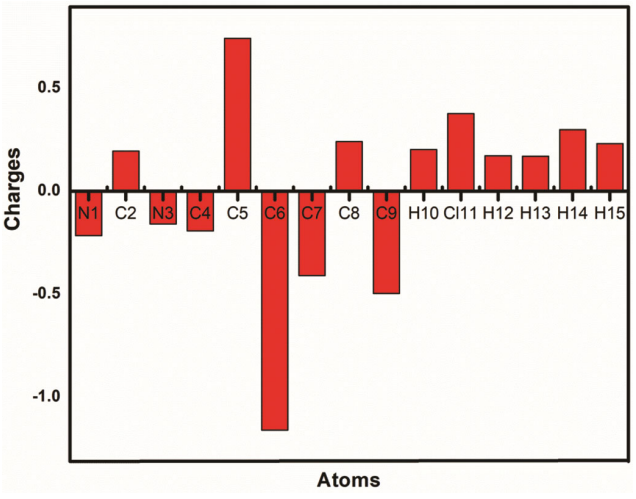

Fig. 7 — Mulliken charges plot for 5-chlorobenzamidazole

Table 7 — Mulliken atomic charge for 5-chlorobenzamidazole

Atoms	Atomic Charges (Mulliken) B3LYP/6-311++G(d,p)
N1	-0.21568
C2	0.195662
N3	-0.15869
C4	-0.19272
C5	0.742644
C6	-1.15987
C7	-0.40897
C8	0.240651
C9	-0.49609
H10	0.202974
Cl11	0.37728
H12	0.17255
H13	0.169452
H14	0.29913
H15	0.231678

$$f_k^0 = \frac{1}{2}[q_j(N+1) - q_j(N-1)]$$

Here, f_k^+ nucleophilic, f_k^- electrophilic and f_k^0 free radical functions on the reference molecule. The atomic charge at the jth atomic site in neutral (N), cationic (N-1), and anionic (N+1) chemical species is indicated by the symbol q_j in these equations. A dual descriptor $\Delta f(r)$ has recently been planned by Morell *et al.*[36] and the equation specifies it as the distinction between the electrophilic and nucleophilic Fukui functions,

$$\Delta f(r) = f_k^+ - f_k^-$$

At a specific location with their sign, the dual descriptor $\Delta f(r)$ clearly distinguishes between nucleophilic and electrophilic attack. In this study, the nucleophilic sites for 5CBZ are N1, N3, C5, C6, C8, H10, H11, H13, and H14 based on the values presented in (Table 8), which meet the requirements for the dual descriptor. Instead, the electrophilic sites C2, C4, C7, C9, H12, and H15 have negative values. Its local behaviour determines how the molecule 5CBZ responds to both electrophilic and nucleophilic attack throughout the process.

Molecular electrostatic potentials (MEP)

To ascertain drug-receptor interactions in biochemistry, MEP mapping utilizing DFT techniques might be helpful. The MEP is connected to the chemically active regions of a molecule, and it also increases awareness of molecular reactivity, substituent effects, electrophilic reactions, and inter and intramolecular connections[37]. Red, yellow, blue, and green have progressively higher electrostatic potential. Here, the blue (electron deficient) area of the molecule was bounded by hydrogen atoms, while the red (electron rich) and somewhat yellow (electron rich) regions of the molecule are caused by the lone pair of nitrogen atoms. This has happened as a result of the hydrogen atoms connection to the electronegative nitrogen atom. Over the ring's system, the neutral electrostatic potentials (green) are encircling. As a result, Figure 8 shows the MEP surfaces of 5CBZ that were estimated at B3LYP/6-311++G(d,p). In this study, the red color patches with

Table 8 — Fukui functions from Mulliken charges for 5-chlorobenzamidazole

Atoms	Mulliken Charges			Fukui functions			
	q(N+1)	q(N)	q(N-1)	f_k^+	f_k^-	f_k^0	$\Delta f(r)$
N1	-0.2124	-0.21568	0.128943	0.003286	-0.34463	-0.17067	0.347916
C2	-0.05947	0.195662	0.24114	-0.25513	-0.04548	-0.15031	-0.20965
N3	-0.21059	-0.15869	-0.01054	-0.0519	-0.14814	-0.10002	0.09624
C4	-0.35328	-0.19272	-0.06802	-0.16056	-0.12471	-0.14263	-0.03585
C5	0.860205	0.742644	0.648161	0.117561	0.094483	0.106022	0.023078
C6	-1.19627	-1.15987	-1.11553	-0.0364	-0.04434	-0.04037	0.00794
C7	-0.56785	-0.40897	-0.33702	-0.15887	-0.07195	-0.11541	-0.08692
C8	0.25745	0.240651	0.259947	0.016799	-0.0193	-0.00125	0.036099
C9	-0.46842	-0.49609	-0.52641	0.027664	0.030317	0.028991	-0.00265
H10	0.12633	0.202974	0.282301	-0.07664	-0.07933	-0.07799	0.00269
C11	0.233931	0.37728	0.597855	-0.14335	-0.22058	-0.18196	0.07723
H12	0.101142	0.17255	0.236819	-0.07141	-0.06427	-0.06784	-0.00714
H13	0.099295	0.169452	0.246964	-0.07016	-0.07751	-0.07383	0.00735
H14	0.23548	0.29913	0.364948	-0.06365	-0.06582	-0.06473	0.00217
H15	0.15444	0.231678	0.30832	-0.07724	-0.07664	-0.07694	-0.0006

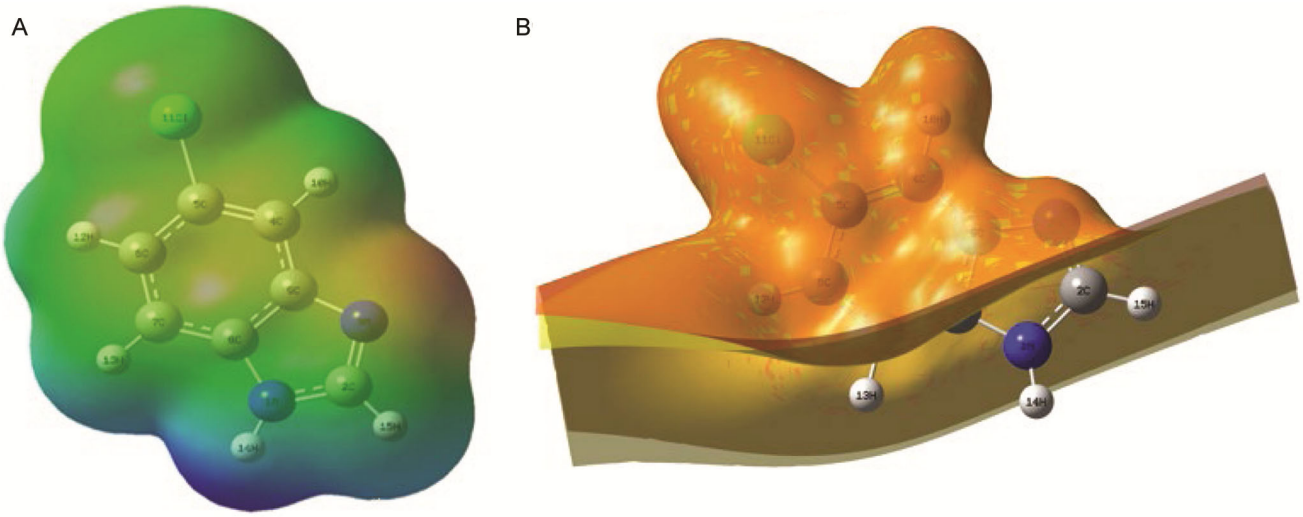

Fig. 8 — (A) MEP; and (B) ESP plot for 5-chlorobenzamidazole

the highest potential make the electrophilic nature of the nitrogen atom (N3) clear. All hydrogens (blue area) are grouped with nucleophilic regions, but particularly hydrogen linked to nitrogen (H14). Similar to how the negative electrostatic potential (ESP), which is revealed by means of a yellowish blob over the chlorine atom, is confined; the positive ESP is concentrated over the remaining part of the molecule. Due to the correlation between ESP, electronegative and partial charges, this outcome is predicted.

Nuclear magnetic resonance (NMR) analysis

To identify the structure of large macromolecules, NMR modeling is a potential method. By means of the DFT/ B3LYP/ 6-311++G(d,p) with GIAO technique[38], the calculated ^{13}C and ^{1}H NMR chemical shifts of 5CBZ are presented in (Table 9). Figure 9 shows the computed ^{13}C and ^{1}H NMR spectra as a plot. The greatest calculated ^{13}C NMR shift for C2 is 166.96 ppm, which is the result of nitrogen's (N1 and N3 atoms) least effective shielding. Because the neighboring carbon nuclei (C6 and C8) have a stronger shielding effect, the carbon atom C7 connected to the ring exhibits a little chemical shift at 115.53 ppm. When hydrogens are joined directly or positioned close to an atom that accepts electrons, their shielding is reduced and a greater wavenumber results from resonance. Therefore, as shown in Figure 9, the estimated signal of H14 connected close to the nitrogen atom (N1) has an extreme value of 10.09 ppm. When hydrogens are positioned closer to an electron donor, the shielding increases, and hence there is a decrease in chemical shift. Because of the connection of the electronegative element (C6), the expected shift values for H12 are 7.14 ppm, as shown in (Table 9).

Cytotoxicity analysis

MCF-7 breast cancer cell lines were obtained from the National Centre for Cell Sciences (NCCS) in Pune, India. DMEM (Dulbecco's Modified Eagle Media) and 10% FBS (Fetal Bovine Serum) were used to keep the cell line alive. To avoid bacterial contamination, the medium was treated with tetracycline (100 g/mL) and penicillin (100 U/mL). The cell lines' medium was maintained at 37°C in a humid atmosphere with 5% CO_2.

The yellow 3-4,5dimethylthiozol-2-Yl)-2,5diphenyl-tetrazoliumbromide (MTT) is reduced by the mitochondrial dehydrogenase of living cells, yielding a visible purple formation product. In live cells, NADPH-dependent reductase is present, which converts the MTT reagent into formazan, a deep purple material. The formazan crystals are then dissolved in the solubilizing solution, and the absorbance at 500-600 nm is measured using a plate reader. 50 mg of MTT dye was dissolved in 10 mL of phosphate buffered saline (PBS). After 1 min of

Table 9 — ^{13}C and ^{1}H NMR chemical shifts for 5-chlorobenzamidazole

^{13}C Assignment	Calculated shift (ppm)	^{1}H Assignment	Calculated shift (ppm)
C7	115.53	H12	7.14
C4	124.01	H13	7.61
C6	125.95	H10	8.21
C5	144.15	H15	9.27
C8	149.59	H14	10.09
C9	159.16		
C2	166.96		

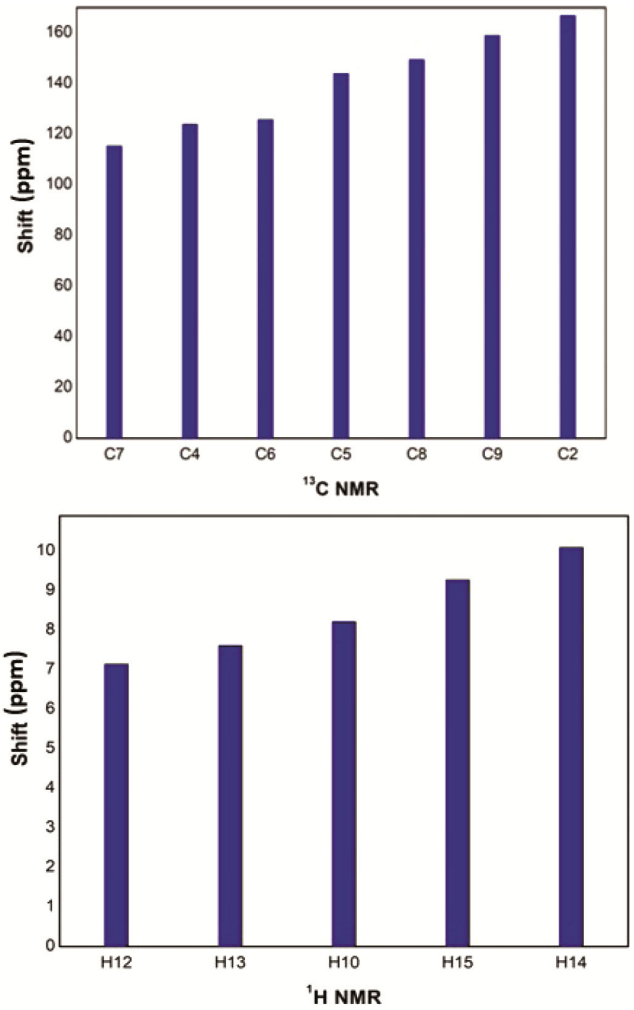

Fig. 9 — ^{13}C and ^{1}H NMR plot of 5-chlorobenzamidazole

vortexing, it was filtered through 0.45 micro filters. MTT was light-sensitive, to keep light out, the container was covered with aluminum foil. The preparation was maintained in a 4°C freezer. To examine sample 5CBZ's anti-cancer efficacy, these MCF-7 cells were visible to various doses of the substance.

For that, live MCF-7 cells were taken out and counted using a hemocytometer. They were then divided into separate 96-well plates after being diluted in DMEM medium to a density of 1×10^4 cells/mL. After that, the cells were cultured for 24 h to facilitate adherence[39]. Then, MCF-7 cells were subjected to control and various doses of 5CBZ (5-20 µg/mL), they were placed in each well. MCF-7 cells were cultured for 24 h at 37°C in a chamber that contained 5% CO_2 and 95% humidified air. After the drug-containing cells had been incubated, the MTT (5 mg/mL in PBS) dye was applied to each well, and they were then washed with new culture media and left to continue incubating for an extra 4 h at 37°C. Cell viability was determined using a multi-well plate reader and absorbance at 540 nm and 100 µL of pure DMSO were used to dissolve the purple formazan that had precipitated. The percentage of stable cells in comparison to the control was used to express the results. Photomicrograph (20x) depicts morphological alterations in MCF-7 cells brought on by sample 5CBZ treatment (5-20 µg/mL for 24 h), including contraction, detachment, blebbing and deformed shape as matched to control. Control cells exhibited typical intact morphology and were photographed using a light microscope. Figure 10 displays the morphological alterations and percentage of cell survival at various doses of 5CBZ against breast cancer MCF-7 cells. The half maximum inhibitory concentrations (IC_{50}) values were calculated and the optimal dosages at various periods were analyzed.

$$\text{Ihibitory of cell proliferation (\%)} = \frac{\text{Mean absorbance of the control} - \text{Mean absorbance of the sample}}{\text{Mean absorbance of the control}}$$

The dose-dependent procedure used to get the IC_{50} values resulted in a 50% reduction in cytotoxicity comparative to control cells. Each experiment was repeated at least three times. Due to its low IC_{50} value, the sample 5CBZ demonstrated strong activity against the MCF-7 (breast cancer cell line). The IC_{50} value of 5CBZ with MCF-7 is 16.82 µg/mL, which is in line with other related benzimidazole compounds[10,11,27] and the standard drug doxorubicin[40], which has an IC_{50} value of 26.1 µg/mL. The one-way analysis of variance (ANOVA) test was used to statistically confirm the cell viability. It is common practice to use a p-value of 0.05 or less to denote statistical significance in the observed data. Table 10 displays the statistical features and mean (%) of cell viability for 5CBZ. According to the study,

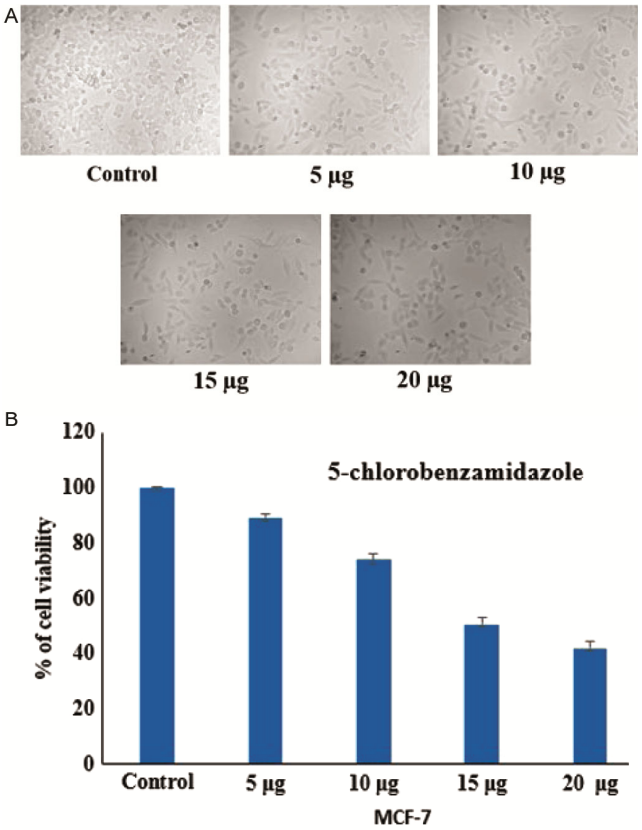

Fig. 10 — (A) Morphological changes; and (B) % of cell viability for different concentrations of 5-chlorobenzamidazole against breast cancer MCF-7 cells

Table 10 — Mean (%) of cell viability with standard deviation for 5-chlorobenzimidazole against MCF-7 cell line

Concentration of sample	Cell line	Mean (%) of cell viability± standard deviation of three independent experiments
5 µg/mL	MCF-7	89.11±1.56
10 µg/mL		73.81±2.12
15 µg/mL		50.68±2.57
20 µg/mL		42.01±2.30
25 µg/mL		23.98±2.34

there is a statistically significant difference ($P = 0.0094$) in the sample averages for values between 5 and 25 μg/mL.

Antibacterial activity

Gram-positive bacteria like *Methicillin Resistant Staphylococcus aureus* (MRSA) and Vancomycin-Resistant Enterococcus faecium (VREF) in addition to Gram-negative bacteria like Serratia were used to evaluate 5CBZ's antibacterial abilities. Pre-cultured in Nutrient Agar (NA) medium, Gram-negative and Gram-positive bacteria were cultured on a rotating shaker at 37°C for an overnight period. The antibacterial activity of various doses of 5CBZ was screened using the agar well diffusion technique. In the middle of a sterile Petri plate, 1 mL of new bacterial culture was pipetted. After that, the Petri plate was filled with sterile Muller Hinton Agar (MHA) and allowed to solidify. After solidifying, 6 mm diameter sterile cork borer holes were drilled into agar plates containing inoculums. Then, a plate containing MHA had bacteria put on it, which was then let to dry. On the other hand, the sample 5CBZ was dissolved in 50% DMSO (Dimethyl sulfoxide) at 0.6 mg/mL as standard solution of 100 μL, and each concentration was added in three separate wells. After that, the plates were incubated at 37°C for 18 h. The inhibition zone, which comprised the diameter of the wells after incubation, was assessed to determine antibacterial activity.

The zone of inhibition (mm) for 5CBZ's antibacterial activity[41,42] was reported in (Table 11 and Fig. 11). *Methicillin-Resistant Staphylococcus aureus* (MRSA) and *Staphylococcus aureus* (*S. aureus*) are tried at various concentrations of the sample 5CBZ (ranging from 25 to 100 μg/mL) as well as Serratia, a gram-negative bacterium. The relationship between this concentration and microbial growth is that the stronger the antibacterial activity of the molecule, the lower the concentration. The bacteria are more susceptible to the antibiotic in the disk if there is a greater zone of inhibition surrounding it. Inhibition zones of 5CBZ have been shown to expand with concentration, acting as a most potent effectiveness against *Staphylococcus aureus*, MRSA and Serratia (Table 11 and Fig. 11). Hence, in terms of zone of inhibition (mm) for MRSA, *S. aureus*, and Serratia, the sample 5CBZ have greater antibacterial activity.

Molecular docking analysis

A computer method called molecular docking is utilized in drug development to look into the binding sites of proteins and ligands[43]. Our in-silico research showed that 5CBZ interacts with proteins that are identified to be related with breast cancer, including

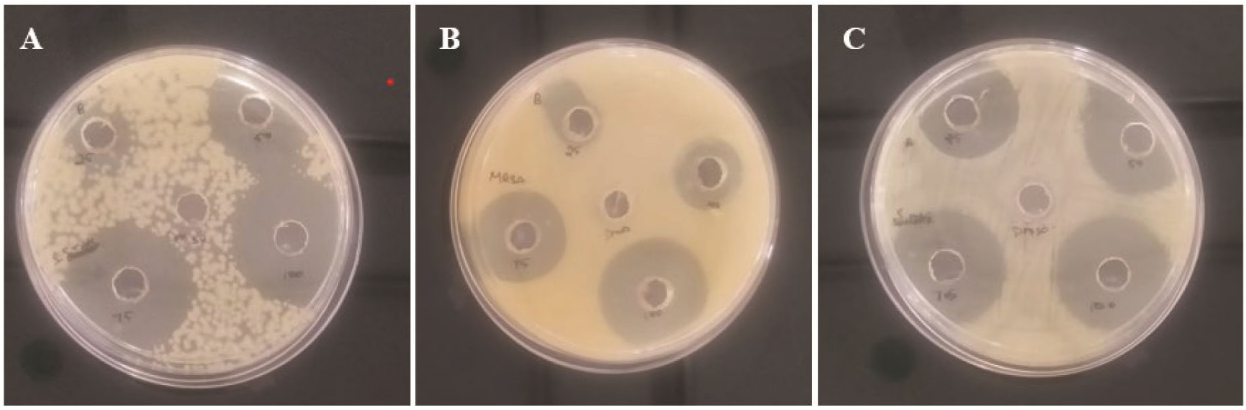

Fig.11 — Inhibition zone representation of different bacteria treated with 5-chlorobenzamidazole: (A) *Staphylococcus aureus*; (B) *Methicillin-resistant Staphylococcus aureus*; and (C) Serratia

Table 11 — Antibacterial analysis of 5-chlorobenzamidazole with various bacteria

5-chlorobenzamidazole Concentration (μg/mL)	Zone of Inhibition (mm)		
	Staphylococcus aureus	*Methicillin-resistant Staphylococcus aureus*	Serratia
25	2	3	4
50	6	5	6
75	8	7	7
100	10	9	9

human progesterone (PDB ID: 1A28) receptor, epidermal growth factor (PDB ID: 1M17) receptor, human estrogen (PDB ID: 1ERE) receptor, and estrogen sulfotransferase (PDB ID: 1AQU) receptor (Figs 12 and 13). Table 12 shows the binding energies of these proteins. Our research demonstrates that the H-bonding residues ARG A: 130, GLY A: 259, and SER A: 138 provide the protein 1AQU and 5CBZ with the greatest amount of contact. The estimated binding free energy is -6.4 Kcal mol^{-1}. Additionally, the current study found that 5CBZ binds to protein 1A28 more strongly at GLN A: 725 and LEU A: 718 with a binding energy of -5.6 $Kcalmol^{-1}$. Similar to

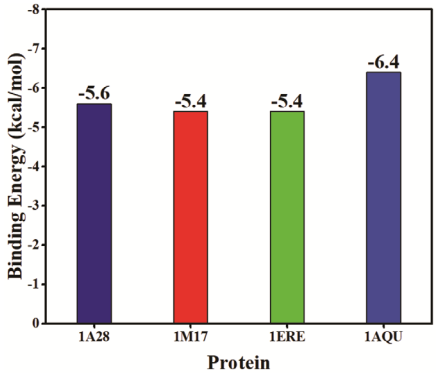

Fig. 12 — Comparison of binding energy of 5-chlorobenzamidazole with 1A28, 1M17, 1ERE and 1AQU

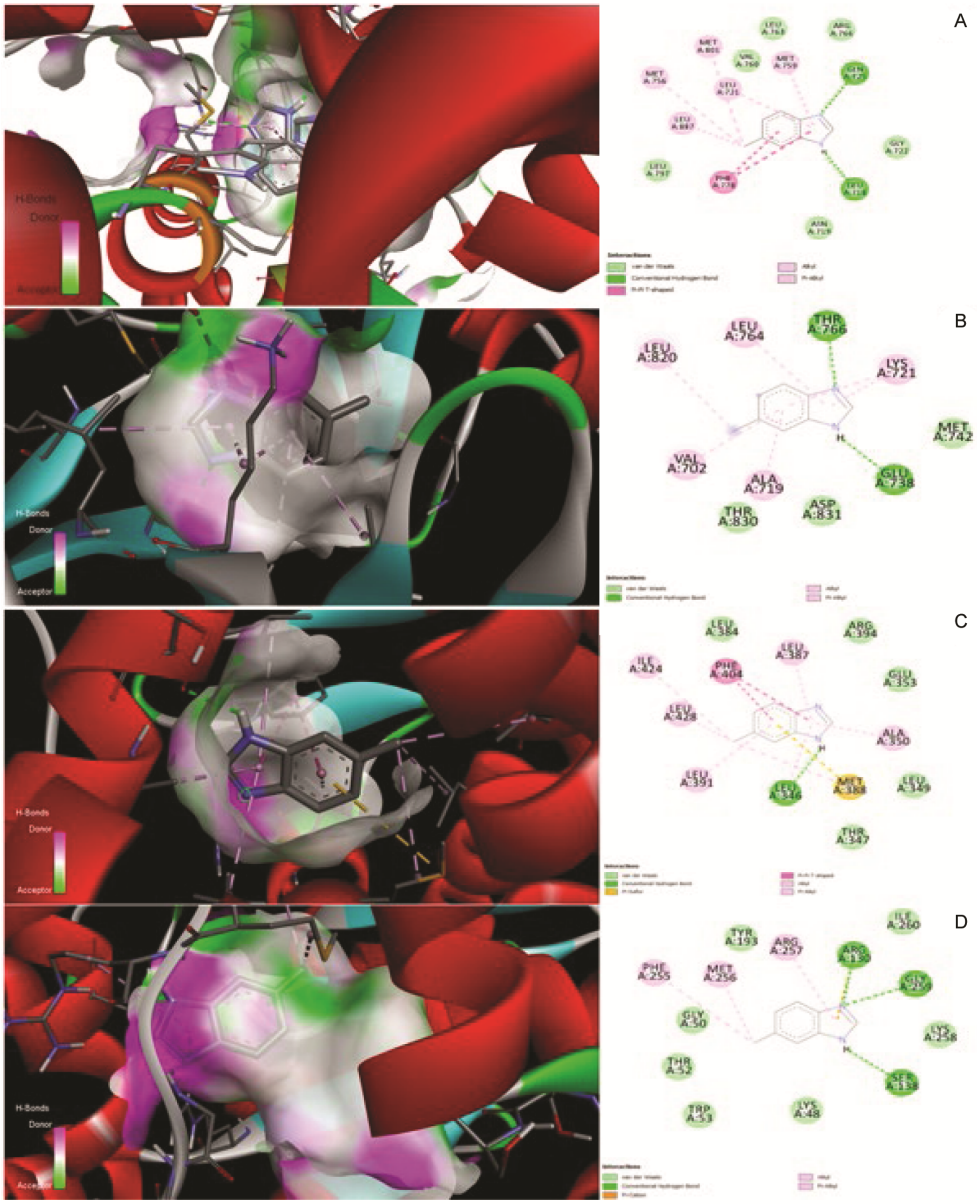

Fig. 13 — Interaction of 5-chlorobenzamidazole with (A) 1A28; (B) 1M17; (C) 1ERE; and (D) 1AQU

Table 12 — Comparison of binding energy of 5-chlorobenzamidazole with 1A28, 1M17, 1ERE and 1AQU along with interacting residues

S. No	Protein	Binding Energy (Kcal/mol)	Interacted Residues	Ligand and Protein atom involved in H-bonding
1	Human Progesterone Receptor (1A28)	-5.6	GLN A:725, LEU A:718, GLY A:722, ASN A:719, PHE A:778, LEU A:797, MET A:756, LEU A:887, MET A:801, LEU A:721, VAL A:760, MET A:759, LEU A:763, ARG A:766	GLN A:725, LEU A:718
2	Epidermal Growth Factor Receptor (1M17)	-5.4	THR A:766, GLU A:738, LEU A:820, LEU A:764, LYS A:721, METY A:742, ASP A:831, ALA A:719, THR A:830, VAL A:702	THR A:766, GLU A:738
3	Human Estrogen Receptos (1ERE)	-5.4	LEU A:346, MET A:388, LEU A;349, THR A:347, ALA A:350, GLU A:353, ARG A:394, LEU A:387, PHE A:404, LEU A:384, ILE A:424, LEU A:428, LEU A:391	LEU A:346
4	Estrogen Sulfotransferase Receptor (1AQU)	-6.4	ARG A:130, GLY A:259, SER A:138, ILE A:260, LYS A:258, LYS A:48, ARG A:257, TYR A:193, MET A:256, PHE A:255, GLY A:50, THR A:52, TRP A:53	ARG A:130, GLY A:259, SER A:138

Table 13 — ADMET profile of 5-chlorobenzamidazole

ADMET prediction	Value	ADMET prediction	Value
CaCo-2 permeability (log Papp in 10^{-6} cm/s)	1.479	P-glycoprotein substrate	No
Intestinal absorption (human) (%)	83.496	P-glycoprotein I inhibitor	No
Skin Permeability (log Kp)	-2.735	P-glycoprotein II inhibitor	No
VDss (human) (log L/kg)	-0.05	Total Clearance (log mL/min/kg)	0.859
Fraction unbound (human) (Fu)	0.322	Renal OCT2 substrate	No
BBB permeability (log BB)	0.388	AMES toxicity test	No
CNS permeability (log PS)	-1.99	Max. tolerated dose (human) (log mg/kg/day)	0.14
CYP2D6 substrate	No	hERG I inhibitor	No
CYP3A4 substrate	No	hERG II inhibitor	No
CYP1A2 inhibitior	No	Oral Rat Acute Toxicity (LD_{50}) (mol/kg)	2.787
CYP2C19 inhibitior	No	Oral Rat Chronic Toxicity (LOAEL) (log mg/kg_bw/day)	1.911
CYP2C9 inhibitior	No	Hepatotoxicity	No
CYP2D6 inhibitior	No	Skin Sensitisation	Yes
CYP3A4 inhibitior	No	T.Pyriformis toxicity (log ug/L)	0.284
Carcinogenicity	Non	Minnow toxicity (log mM)	1.612

other breast cancer proteins 1M17 and 1ERE, 5CBZ exhibits strong binding free energies (-5.4 $Kcalmol^{-1}$ and -5.4 $Kcalmol^{-1}$, respectively). Therefore, it seems sense to speculate that the substance 5CBZ may have a dominant anti-breast cancer activity.

ADMET Prediction

Due to poor ADME (absorption, distribution, metabolism, and excretion) qualities, the majority of novel drug candidates fail in clinical trials. These late-stage failures are a major contributing factor to the growing costs of the new pharmaceutical development process. Early detection of poor candidates may significantly cut down on lost time and money while also streamlining the entire development process[44]. As a result, it is critical to analyze the pharmacokinetic features of potential therapeutic candidates as early in the drug development process as possible. The intended characteristics of a specific chemical can be improved by concentrating lead optimization efforts using ADME prediction. The molecule's HIA (Human Intestinal Absorption) score is greater (83.496%), as determined by ADMET properties obtained from the ADMET-SAR service. In humans, the LD_{50} plays a crucial role in predicting the symptoms of poisoning after an acute overdose. The sample 5CBZ had a minimal LD_{50} value of 2.787 mol/kg, and the molecule has a remarkably good (0.388) Blood-Brain Barrier (BBB) penetration rate. In addition, several ADMET parameters were discovered and are displayed in (Table 13). According to these data, 5CBZ has a good plasma protein binding, a positive blood brain barrier crossing (BBB), and a reasonable human intestinal absorption probability.

Conclusion

The DFT/B3LYP/6-311++G(d,p) technique was used to optimize the properties of 5-chlorobenzamidazole. The variations in bond lengths and angles are caused by hyper conjugation between the molecule's chlorine atom, benzene, and imidazole

ring systems. The DFT-B3LYP theory offered an accurate description of the vibrational assignments, which agree with the computed and experimental data. Understanding the molecule's chemical and biological characteristics has been done by looking at its reduced energy gap (5.3589 eV) for HOMO and LUMO, global reactivity descriptors and DOS spectra. Through $\pi \rightarrow \pi^*$ electron delocalization, NBO's result demonstrates the intra and intermolecular charge exchange. The ring and substitution atoms were revealed to be the most likely targets for electrophilic and nucleophilic attacks using Mulliken charge analysis and Fukui functions. The MEP findings represent the molecule's electrophilic (nitrogen) and nucleophilic (hydrogen) reactivity sites. The molecule's proton and carbon NMR shifts have been computed. The docking outcomes showed that the 5CBZ had the strongest binding energy (-6.4 $Kcalmol^{-1}$) when interacting with the estrogen sulfotransferase receptor (PDB ID: 1AQU). Based on its cytotoxicity, anti-bacterial activity, and ADMET analysis, 5CBZ will be an effective anti-breast cancer medicine with minimal adverse effects during medical procedures.

Acknowledgement

The authors would like to thank Kalasalingam Academy of Research and Education's International Research Centre (IRC) for providing funding assistance for the creation of the computational research centre.

Conflict of interest

All authors declare no conflicts of interest.

References

1 Kucuk C, Synthesis, characterization, DFT studies, and molecular docking investigation of silver nitrate complex of 5-benzimidazole carboxylic acid as targeted anticancer agents. *J Mol Struct,* 1293 (2023) 136.

2 Sharma S, Gupta M & Sahu J, Significance of Benzimidazole analogues for the creation of novel molecules in drug discovery. *Curr Chem Lett*, 12 (2023) 27.

3 Ebenezer O, Oyetunde-Joshua F, Omotoso OD & Shapi M, Benzimidazole and its derivatives: Recent Advances (2020-2022). *Results Chem*, 5 (2023) 100925.

4 Pathare B & Bansode T, Biological active benzimidazole derivatives. *Results Chem*, 3 (2021) 100200.

5 Nath J, Paul R, Ghosh SK, Paul J, Singha B & Debnath N, Drug repurposing and relabeling for cancer therapy: Emerging benzimidazole antihelminthics with potent anticancer effects. *Life Sci*, 258 (2020) 118189.

6 Song B, Park EY, Kim KJ & Ki SH, Repurposing of benzimidazole anthelmintic drugs as cancer therapeutics. *Cancers*, 14 (2022) 4601.

7 Nguyen VT, Huynh TKC, HoG TT, Nguyen THA, Nguyen TLA, Dao DQ, Mai TVT, Huynh LK & Hoang TKD, Metal complexes of benzimidazole-derived as potential anti-cancer agents: Synthesis, characterization, combined experimental and computational studies. *R Soc Open Sci*, 9 (2022) 220659.

8 Haider K & Yar MS, Advances of benzimidazole derivatives as anticancer agents: bench to bedside. *Intech Open Ltd*, London. 2022.

9 Venugopal S, Kaur B, Verma A, Wadhwa P, Magan M, Hudda S & Kakoty V, Recent advances of benzimidazole as anticancer agents. *Chem Biol Drug Des*, 102 (2023) 357.

10 Lee YT, Tan YJ & Oon CE, Benzimidazole and its derivatives as cancer therapeutics: The potential role from traditional to precision medicine. *Acta Pharm Sin B*, 13 (2023) 478.

11 Kunjumol VS, Jeyavijayan S, Sumathi S & Karthik N, Spectroscopic, computational, cytotoxicity, and docking studies of 6-bromobenzimidazole as anti-breast cancer agent. *J Mol Recognit*, 37 (2024) e3074.

12 Becke AD, Density-functional thermochemistry. III. The role of exact exchange. *J Chem Phys,* 98 (1993) 5648.

13 Daghar C, Issaoui N, Roisnel T, Dorcet V & Marouani H, Empirical and computational studies on newly synthesis cyclohexylammonium perchlorate. *J Mol Struct*, 1230 (2021) 129820.

14 Frisch MJ, Trucks GW, Schlegel HB, Scuseria GE, Robb MA, Cheeseman JR, Scalmani G, Barone V, Petersson GA, Nakatsuji H, Li X, Caricato M, Marenich A, Bloino J, Janesko BG, Gomperts R, Mennucci B, Hratchian HP, Ortiz JV, Izmaylov AF, Sonnenberg JL, Williams-Young D, Ding F, Lipparini F, Egidi F, Goings J, Peng B, Petrone A, Henderson T, Ranasinghe D, Zakrzewski VG, Gao J, Rega N, Zheng G, Liang W, Hada M, Ehara M, Toyota K, Fukuda R, Hasegawa J, Ishida M, Nakajima T, Honda Y, Kitao O, Nakai H, Vreven T, Throssell K, Jr. Montgomery JA, Peralta JE, Ogliaro F, Bearpark M, Heyd JJ, Brothers E, Kudin KN, Staroverov VN, Keith T, Kobayashi R, Normand J, Raghavachari K, Rendell A, Burant JC, Iyengar SS, Tomasi J, Cossi M, Millam JM, Klene M, Adamo C, Cammi R, Ochterski JW, Martin RL, Morokuma K, Farkas O, Foresman JB & Fox DJ, Gaussian, Inc., Wallingford CT, 2016. Gaussian 09. 2013 Gaussian 09, Revision A.02, Gaussian, Inc., Wallingford CT.

15 Young DC. Computational chemistry: a practical guide for applying techniques to real world problems. *John Wiley & Sons Ltd*, *New York*, 2001.

16 Sundius T. Molvib (V. 70): calculation of harmonic force fields and vibrational modes of molecules. *QCPE Program*, 807 (2002).

17 Oboyle NM, Tenderholt AL & Langner KM, Cclib: a library for package-independent computational chemistry algorithms. *J Comput Chem*, 29 (2008) 839.

18 Lakka NS, Kuppan C, Vadagam N, Ravinathan P, Chepuri K & Sanjeeva R, Molecular docking, in-vitro anticancer evaluation and ADME profiling of 7-Oxo Midostaurin. *J Mol Struct*, 1293 **(**2023**)** 136159.

19 Biovia DS. BIOVIA Discovery Studio 2017 R2: A comprehensive predictive science application for the Life Sciences. San Diego, CA, USA. 2017.

20 Kim S, Thiessen PA, Bolton EE, Chen J, Fu G, Gindulyte A, Han L, He J, He S, Shoemaker BA, Wang J, Yu B, Zhang J & Bryant SH, PubChem substance and compound databases. *Nucleic Acids Res*, 44 (2016) D1202.

21 Trott O & Olson AJ, AutoDock Vina: improving the speed and accuracy of docking with a new scoring function, efficient optimization, and multithreading. *J Comput Chem*, 31 (2009) 455.

22 Jia CY, Li JY, Hao GF & Yang GF, A drug-likeness toolbox facilitates ADMET study in drug discovery. *Drug Discov Today*, 25 (2020) 248.

23 Muthunatesan S & Ragavendran VA, A study of vibrational spectra and investigations of charge transfer and chemical bonding features of 2-chloro benzimidazole based on DFT computations. *Spectrochim Acta A Mol Biomol Spectrosc*, 134 (2015) 148.

24 Panneerselvam K & Garcla MS, 2-chlorobenzimidazole. *Acta Crystallogr*, C52 (1996) 1799.

25 Jeyavijayan S. Molecular structure, vibrational spectra, NBO analysis, first hyperpolarizability, and HOMO–LUMO studies of 2-amino-4-hydroxypyrimidine by density functional method. *J Mol Struct*, 1085 (2015) 137.

26 Jeyavijayan S & Arivazhagan M, FTIR, FT-Raman spectra and DFT analysis of m-nitrobenzaldehyde oxime. *Indian J Pure Appl Phys*, 50 (2012) 623.

27 Kunjumol VS, Jeyavijayan S, Karthik N & Sumathi S, Spectroscopic, computational, docking and cytotoxicity studies on 2-(2-chlorophenyl) benzimidazole as a potent anti-breast cancer agent. *Indian J Pure Appl Phys*, 62 (2024) 576.

28 Socrates G, Infrared and Raman characteristic group frequencies. *John Wiley & Sons, New York*, 2001.

29 Ramuthai M, Jeyavijayan S, Premkumar R & Uma Priya M, Structure spectroscopic investigation molecular docking and *in vitro* cytotoxicity studies on 4,7- dihydroxycourmin:A breast cancer drug. *J Comput Biophys Chem*, 21 (2022) 219.

30 Marinho MM, Almeida-Neto FWQ, Marinho EM, Silva LPD, Menezes, RRPPB, Dos Santos RP, Marinho ES, de Lima-Neto P & Martins AMC, Quantum computational investigations and molecular docking studies on amentoflavone. *Heliyon*, 7 (2021) e06079.

31 Khalid M, Anwer W, Adeel M, Shafiq Z, Braga AAC, Assiri MA, Imran M & Ullah A, Exploration of the interesting photovoltaic behavior of the fused benzothiophene dioxide moiety as a core donor with modification in acceptors for high-efficacy organic solar cells. *RSC Adv*, 2 (2022) 29010.

32 Diwaker. Spectroscopic (FT-IR, H-1, C-13 NMR, UV), DOS and orbital overlap population analysis of copper complex of (E)-4-(2-(4-nitrophenyl) diazenyl)-N, N bis ((pyridin-2-yl) methyl) benzamine by density functional theory. *Spectrochim Acta A Mol Biomol Spectrosc*, 136 (2015) 1932.

33 Anitha K, Balachandran V, Narayana B & Raja B, Molecular orbital analysis, vibrational spectroscopic investigation, static and dynamic NLO responses of Ethyl 6-nitro-1H-indole-3-carboxylate. *Mater Res Innov*, 22 (2018) 333.

34 Pramoth B, Naresh P, Naveen S, Loganth NK, Ganguly S, Panda J, Murugesan S, Raghu AV & Warad I, Synthesis, spectral characterization, crystal structure and theoretical investigation of (E)-3-(4-bromothiophen-2-yl)-1-(5-bromothiophen-2-yl) prop-2-en-1-one. *Chem Data Collect*, 31 (2021) 100587.

35 Ayers PW & Parr RG, Variational principles for describing chemical reactions: the Fukui function and chemical hardness revisited. *J Am Chem Soc*, 122 (2000) 2010.

36 Morell C, Grand A & Toro-Labbe V, New dual descriptor for chemical reactivity. *J Phys Chem A*, 109 (2005) 205.

37 Aman H, Rashid N, Ashraf Z, Bibi A, Chen HT & Sathishkumar N, Synthesis, density functional theory (DFT) studies and urease inhibition activity of chiral benzimidazoles. *Heliyon*, 6 (2020) e05187.

38 Fizer M, Slivka M, Korol N & Fizer O, Identifying and explaining the regioselectivity of alkylation of 1, 2, 4-triazole-3-thiones using NMR, GIAO and DFT methods. *J Mol Struct*, 1223 (2021) 128973.

39 Christopher Jeyaseelan S & Benial AMF, Spectroscopic characterization, DFT studies, molecular docking and cytotoxic evaluation of 4-nitro-indole-3-carboxaldehyde: a potent lung cancer agent. *J Mol Recognit*, 34 (2021) e2872.

40 Batran RZ, Kassem AF, Abbas EMH, Elseginy SA & Mounier MM, Design, synthesis and molecular modeling of new 4-phenylcoumarin derivatives as tubulin polymerization inhibitors targeting MCF-7 breast cancer cells. *Bioorg Med Chem*, 26(12) (2018) 3474.

41 Ramaswamy S, Kongara D, Dwarampudi LP & Gade R, Synthesis, spectral characterization, anti-bacterial, cytotoxic evaluation and docking studies of new urea and thiourea derivatives. *Indian J Biochem Biophys*, 59 (2022) 767.

42 Sharma V, Sharma S, Mehra R, Kapoor KK, Dhar MK & Kaul S, Anti-bacterial activity of neoandrographolide derivatives: In silico interaction with the bacterial target. *Indian J Biochem Biophys,* 59 (2022) 157.

43 Karthik N, Jeyavijayan S & Sumathi S, Docking studies, molecular structure, and spectroscopic analysis of 3-chlorobenzamide as an anti-cancer agent. *Indian J Biochem Biophys*, 61 (2024) 204.

44 Trilaksana H. ADMET, Pharmacokinetic and Docking properties of the fungal drug 2-(2, 4-difluorophenyl)-1, 3-bis (1, 2, 4-triazol-1-yl) propan-2-ol by using Quantum computational methods. *Indian J Biochem Biophys*, 60 (2022) 58.